THE ASTROPHYSICAL JOURNAL, 472:327–340, 1996 November 20

A GRID OF MODEL ATMOSPHERES AND SYNTHETIC SPECTRA FOR THE FAR-ULTRAVIOLET ANALYSIS OF OLD STELLAR POPULATIONS

THOMAS M. BROWN
Department of Physics and Astronomy, Johns Hopkins University, Charles and 34th Streets, Baltimore, MD 21218
HENRY C. FERGUSON
Space Telescope Science Institute, 3700 San Martin Drive, Baltimore, MD 21218
AND
ARTHUR F. DAVIDSEN
Department of Physics and Astronomy, Johns Hopkins University, Charles and 34th Streets, Baltimore, MD 21218
Received 1996 April 19; accepted 1996 June 21

ABSTRACT

We present a grid of stellar synthetic spectra suitable for detailed comparison to far-ultraviolet (FUV) observations obtained with the Hopkins Ultraviolet Telescope (HUT), *IUE*, and *Hubble Space Telescope* (*HST*). Our specific application is to study the hot stellar populations in elliptical galaxies, but we anticipate that the models will be useful for other purposes. The 1497 spectra span a range of 10,000 K $\leq T_{\rm eff} \leq$ 250,000 K and $2 \leq \log g \leq 8.5$, with three metallicities: $Z = Z_\odot$, $Z = 0.1\ Z_\odot$, and $Z = 0.01\ Z_\odot$. A variety of simplifying assumptions have been made to reduce computer time and improve convergence, at the inevitable expense of some accuracy. Nevertheless, models in the grid reproduce the overall continuum shape and most of the absorption features seen in HUT spectra of four evolved stars at temperatures of 17,000, 29,900, 36,100, and 55,000 K. The most serious discrepancy is in the cores of the Lyman series lines, where the observed lines are not as deep as those obtained from the models. Until this problem is resolved, the Lyman series lines will not provide a very accurate measure of $T_{\rm eff}$ or $\log g$.

While the synthetic spectra in this grid may not be appropriate for detailed analysis of high signal-to-noise ratio stellar spectra, they are sufficiently similar to the observed stars to provide a considerable advantage over existing models for the analysis of the FUV spectra of composite systems, such as elliptical galaxies and globular clusters, where the advantages of having a large, well-sampled grid of models tend to outweigh the known inadequacies of the individual grid points.

Subject headings: stars: abundances — stars: atmospheres — stars: early-type — stars: horizontal-branch — ultraviolet: stars

1. INTRODUCTION

The utility of elliptical galaxies for carrying out fundamental measurements of the age and geometry of the universe has been recognized for decades. However, uncertainties in the chemical composition of elliptical galaxies and the evolution of their stellar populations currently undermines most of these tests. A specific issue is the source of the observed far-ultraviolet (FUV) flux, which could be either an evolved population with low metallicity (see Lee 1994) or high metallicity (see Bressan, Chiosi, & Fagotto 1994). In order to understand these stellar populations, we must extend our spectroscopic information shortward of Lyα λ1216, down to the Lyman limit at 912 Å. The answer to the metallicity debate lies in this FUV regime.

In March of 1995, the Hopkins Ultraviolet Telescope (HUT) was flown aboard the Space Shuttle Endeavour during the Astro-2 mission. It collected FUV spectra of six elliptical and S0 galaxies, covering the wavelength range from 820 to 1840 Å with a resolution of 2–4 Å. In order to model the stellar populations of these galaxies, we integrate individual synthetic spectra for the stars comprising a given population and compare the integrated model to the HUT data. The database of synthetic spectra that currently enjoys the most use is the Kurucz (1993) atlas, and we used this database for our continuum study of the HUT galaxies (Brown, Ferguson, & Davidsen 1995). While this atlas is of great utility to the astrophysics community, it has certain limitations that make it unsuitable for the detailed analysis of HUT spectra: the assumption of local thermodynamic equilibrium (LTE) for the stellar atmospheres, and a resolution of only 10 Å in the synthetic spectra.

Using the codes of Hubeny (1988), we have computed a grid of stellar atmospheres and synthetic spectra covering the wavelength range from 900 to 1800 Å with a resolution of 3 Å. These models were computed for comparison to the HUT data for early-type galaxies and are not meant for use as a high-precision database of synthetic spectra. To produce the hundreds of grid points that are needed for our stellar population models, we trade off some accuracy in the models in order to reduce computer time and convergence problems for the atmospheres. In this paper, we compare models to HUT data for several stars in order to demonstrate the advantages and limitations of our grid. A subsequent paper will apply this grid to the HUT data for elliptical galaxies.

2. THE GRID

Our grid of 1497 synthetic spectra includes the range of temperatures and gravities that are expected for horizontal-branch (HB) stars and their progeny, as determined from the evolutionary tracks of Dorman, Rood, & O'Connell (1993) and Vassiliadis & Wood (1994). The temperature ranges from 10,000 to 250,000 K, with an irregular spacing that varies from 500 to 25,000 K in order to minimize the percentage error when integrating the synthetic spectra into composite models. Although the accuracy of the synthetic spectra varies, they are most accurate for temperatures below 60,000 K; stars in this temperature range dominate

the FUV flux of early-type galaxies (see Brown et al. 1995). The surface gravity for the atmospheres ranges from log $g = 2$ to 8.5, with a spacing of 0.5 for $T_{\rm eff} < 20{,}000$ and 0.25 for $T_{\rm eff} \geq 20{,}000$ K. There are also three metallicities: $Z = Z_\odot$, $Z = 0.1\ Z_\odot$, and $Z = 0.01\ Z_\odot$. Figure 1 shows the evolutionary tracks and our grid points.

3. MODEL ATMOSPHERES

3.1. *The Classical Model Atmosphere Problem*

The computation of a classical stellar atmosphere (see Hubeny 1988) involves solving the basic equations that determine its physical structure while assuming a steady state, plane-parallel, horizontally homogeneous atmosphere. These equations define the physical properties at each layer: radiative transfer determines the mean intensities for a given set of frequencies; hydrostatic equilibrium determines the total particle number density; radiative equilibrium determines the temperature; statistical equilibrium determines the occupation numbers of all explicitly considered atomic energy levels; and charge and particle conservation determine the electron density.

The classical solution makes several simplifying assumptions that reduce an extremely complex problem to manageable dimensions (see Mihalas 1970). The plane-parallel geometry makes the reasonable assumption that the thickness of the atmosphere is a small fraction of the stellar radius. While observations of our own Sun have shown that its atmosphere is not horizontally homogeneous, the assumption of homogeneity in each layer of the atmosphere treats each layer by the average physical properties of that layer. The assumption of a steady state atmosphere implies that all equations and atomic occupation numbers are independent of time and that phenomena such as pulsations, shocks, and variable magnetic fields are absent. Hydrostatic equilibrium assumes there are no velocity fields and that the pressure stratification balances the gravitational field. Radiative equilibrium demands that all energy is transported by radiation, as opposed to convection.

Following the formalism of Hubeny (1988), the model atmosphere is fully described by a set of vectors ψ_d for every depth point in the atmosphere; the depth points run from $d = 1$ to ND. The vector ψ_d is given by (Hubeny & Lanz 1995)

$$\psi_d = \{J_1, \ldots, J_{NF}, N, T, n_e, n_1, \ldots, n_{NL}\} ,$$

where J_i is the mean intensity of radiation in the ith frequency point, N is the total particle number density, T is the temperature, n_e is the electron density, n_j is the population of atomic energy level j of a given element considered in the model, NF is the number of frequency points, and NL is the number of atomic energy levels. The dimension of ψ_d is $NN = NF + NL + 3$.

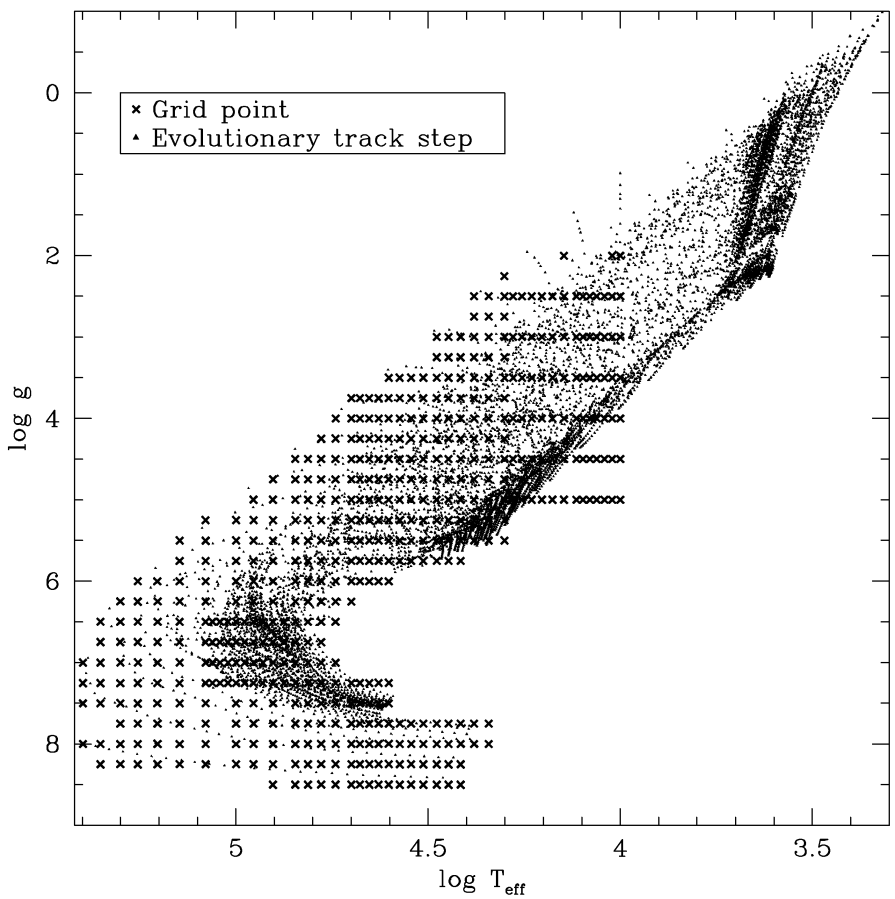

FIG. 1.—Our grid of synthetic spectra (*crosses*) was chosen with the purpose of integrating over stellar evolutionary tracks (Dorman et al. 1993; Vassiliadis & Wood 1994) while minimizing the differences between the track steps (*dots*) and grid points (*crosses*). The density of grid points thus increases as one moves to cooler temperatures but also increases around the concentrated regions of evolutionary track parameter space. Stars below 10,000 K do not contribute significantly to the FUV flux from elliptical galaxies.

A model atmosphere is computed via a series of iterations, proceeding until the fractional change in the physical parameters is small enough to consider the model converged. In general, each iteration consists of a formal solution, which determines the radiation field and level populations, and then linearization, which determines new estimates of the physical variables. Using the method of complete linearization, the computer time for model convergence scales as $N_{\rm iter} \times ND \times NN^3$. An innovation of the latest versions of TLUSTY, the model atmosphere code of Hubeny (1988), is the use of a CL/ALI hybrid scheme. This scheme uses the method of complete linearization (CL) for the most crucial frequency points and the accelerated lambda iteration (ALI) method for the remainder. In the ALI formalism, the radiation intensity is expressed through an approximate lambda operator acting on the source function, plus a corrective term known from the previous iteration. The radiation intensity is thus effectively eliminated from the set of unknown variables. The hybrid CL/ALI method reduces computer time by reducing the number of frequency points that are completely linearized, since the computation time for model atmosphere convergence increases as the number of such frequency points cubed (see Hubeny & Lanz 1995 for a full discussion).

3.2. *The Model Atmospheres of the Grid*

To produce a synthetic stellar spectrum at a point in our grid, we must first have a model atmosphere. The atmosphere comes from two different sources, depending upon the temperature regime. For $T_{\rm eff} \geq 20{,}000$ K, we generate an atmosphere using version 185 of the program TLUSTY (Hubeny 1988; Hubeny & Lanz 1995). For $T_{\rm eff} < 20{,}000$ K, we use Kurucz (1993) LTE atmospheres.

TLUSTY can be used to produce three types of model atmospheres: an LTE-gray atmosphere, an LTE atmosphere, or a non-LTE (NLTE) atmosphere, in which each type is more complex than the previous. Each point in our grid starts with an LTE-gray atmosphere, which makes two simplifying assumptions. The first is that of LTE, which means that the distribution of atoms among their excitation and ionization states is calculated from the local values of two thermodynamic variables: temperature and electron density (see Mihalas 1970). The second assumption is that of the gray atmosphere, in which the opacity is independent of frequency. Once an LTE-gray atmosphere model has converged, we use it as the starting point for calculating an LTE atmosphere (no longer assumed gray). If the grid point has $T_{\rm eff} < 45{,}000$ K, the model atmosphere for that grid point is then finished. If the grid point has $T_{\rm eff} \geq 45{,}000$ K, the LTE model is used as the starting point for a further iteration: the NLTE atmosphere. In the NLTE atmosphere, the equation of state is nonlocal, since the state of the gas and the radiation field are now coupled. Although one can argue for the importance of NLTE effects for $T_{\rm eff}$ greater than 10,000 K (see Hubeny & Lanz 1995 and references therein), we choose to trade off some accuracy in exchange for simpler models by only calculating NLTE models for those grid points with $T_{\rm eff} \geq 45{,}000$ K.

Although we make several simplifying assumptions, the resulting synthetic spectra match observed HUT FUV spectra reasonably well (see § 6). To reduce computation time and convergence problems, the TLUSTY model atmospheres consist only of H and He. This simplification reduced the time for this project from years to months, for two reasons. First, because the computation time for a model atmosphere at best scales linearly with the number of unknowns (frequency points and atomic energy levels) and at worst scales with the number cubed, the cost of additional frequencies and levels from heavier elements would be quite high. Second, the chance of model divergence greatly increases with the number of unknowns. The use of pure H and He atmospheres introduces certain limitations to the accuracy of the models, and these vary according to the temperature regime. For temperatures below 20,000 K, the FUV continuum opacity from metals becomes increasingly important, and these simple TLUSTY atmospheres produce spectra that diverge more and more from reality as one moves to cooler and cooler temperatures, which leads to our use of Kurucz (1993) atmospheres in this regime. For temperatures above 50,000 K, the extreme-ultraviolet (EUV) continuum opacity becomes increasingly important to the temperature structure of the atmosphere, which in turn affects the resulting FUV spectrum. The lack of metals will thus lead to increasing inaccuracy as one moves to hotter temperatures above 50,000 K.

For the LTE-gray and LTE atmospheres, we explicitly consider nine atomic energy levels of H I, 14 levels of He I, and 14 levels of He II. For the NLTE atmospheres, we drop the He I levels, since the temperature regime considered for these atmospheres is above 45,000 K. We compute all allowed transitions between these energy levels. We also assume a depth-independent turbulent velocity of 2 km s^{-1}. The properties of the atmosphere are calculated at 70 depth points. We use a hybrid CL/ALI method (Hubeny & Lanz 1995): the frequency points near the Lyman limit and the transitions between the lowest atomic energy levels are treated using the CL formalism, while the remainder are treated with the ALI formalism. During the atmospheric structure calculation, all line transitions assume Doppler profiles. Stark broadening is an additional option, but its use in the atmosphere calculation increases computation time by a factor of 4, and the effect of its use is small ($\leq 5\%$ variations in the final spectrum). However, Stark broadening is considered for lines in the synthetic spectrum.

4. SYNTHETIC SPECTRA

For the next stage we input a model atmosphere (either from TLUSTY or a Kurucz atmosphere; see Table 1) and line list into the program SYNSPEC (version 36; Hubeny, Lanz, & Jeffery 1995), which solves the radiative transfer equation to produce a synthetic spectrum. Our line list (compiled from those lists provided with the SYNSPEC package) contains 114,799 transitions between 800 and 1900 Å for those atoms with atomic number $Z \leq 28$. If an element was treated in NLTE in the atmosphere, SYNSPEC will also treat the element in NLTE in the spectrum calculation. For those elements that were either treated in LTE in the atmosphere or not explicitly included in the atmosphere, SYNSPEC uses an approximate NLTE

TABLE 1

MODEL ATMOSPHERES USED IN SYNTHETIC SPECTRA CALCULATIONS

Temperature Regime	Atmosphere
10,000 K $\leq T_{\rm eff} <$ 20,000 K	Kurucz 1993 LTE
20,000 K $\leq T_{\rm eff} <$ 45,000 K	TLUSTY LTE
45,000 K $\leq T_{\rm eff} \leq$ 250,000 K.....	TLUSTY NLTE

calculation by means of the second-order escape probability theory (Hubeny et al. 1995).

If the input atmosphere is a TLUSTY atmosphere, we calculate continuum opacities from the atomic energy levels of H and He that were used in the model atmosphere and calculate line opacities from the transitions in the line list. If the input atmosphere is a Kurucz (1993) atmosphere, we add additional continuum opacities from elements other than H and He, since these opacities become important at lower temperatures. The penalty in computation time is now much less for considering these energy levels, since we already have a converged atmosphere model from the Kurucz (1993) database, and we are only computing the emergent synthetic spectrum. We thus include continuum opacity from four levels of C I, eight levels of C II, three levels of N I, 17 levels of N II, three levels of O I, 17 levels of O II, one level of Mg I, three levels of Mg II, eight levels of Al II, eight levels of Al III, two levels of Si I, five levels of Si II, and 23 levels of Si III. Our atomic data for the energy levels and photoionization cross sections come from the TOPbase (Cunto et al. 1993) interface to the Opacity Project database. Because the data in TOPbase are theoretical, small errors in the energy levels cause continuum edges to be shifted by tens of angstroms in the synthetic spectra. To correct these shifts, we have shifted the energy levels and the cross sections using measured energy levels from Musgrove et al. (1996) and Moore (1949). When including the continuum opacities above, we also include opacity from quasi-molecular hydrogen (Allard & Koester 1992), which can become a significant contributor to continuum opacity for models with $T_{\rm eff} < 20{,}000$ K.

SYNSPEC outputs completely resolved synthetic spectra with over 100,000 pixels between 900 and 1800 Å. Line profiles are computed as Voigt functions that take into account the effects of natural, Stark, van der Waals, and thermal Doppler broadening. We convolve these spectra to give them a linear pixel spacing of 0.5 Å and a resolution of 3 Å to match approximately the resolution of HUT spectra. The rotational and instrumental convolution was performed using the ROTIN code that comes with the SYNSPEC package, assuming a FWHM of 3 Å and $v \sin i = 50$ km s^{-1}. Our use of the IRAF fitting routine SPECFIT (Kriss 1994) requires models with a linear wavelength scale, although the HUT data have a slightly nonlinear pixel spacing.

For all of our synthetic spectra, there are inconsistencies between the opacities assumed in the spectra and those assumed for the model atmospheres. For $T_{\rm eff} \geq 20{,}000$ K, we use pure H and He model atmospheres but assume line blanketing from heavier elements when creating the synthetic spectra. For $T_{\rm eff} < 20{,}000$ K, we use Kurucz (1993) model atmospheres, but when creating the synthetic spectra, we assume fewer sources of continuum and line opacity than Kurucz assumed in his atmosphere calculations. These inconsistencies prevent a strict conservation of flux in the output spectra from SYNSPEC but do not significantly diminish the accuracy of their spectral shapes. In other words, the emergent flux $F \neq \sigma T^4$ when F_λ is integrated over all wavelengths, but the deviations in continuum shape from a self-consistent model are only a few percent over the HUT spectral range. Hence, the spectra can simply be renormalized to the proper flux. To correct the absolute fluxes in our synthetic spectra, we renormalize our spectra by comparing our grid to the corresponding spectra in the grids of Kurucz (1992) and Clegg & Middlemass (1987). If there is no corresponding spectrum for comparison, we interpolate or extrapolate from the known corrections. The corrections are largest for our solar metallicity spectra, where, on average, the magnitude of the correction is 20% in the Kurucz (1992) regime ($T_{\rm eff} < 50{,}000$ K) and 10% in the Clegg & Middlemass (1987) regime ($T_{\rm eff} \geq 50{,}000$ K). The corrections are half as large for our lower metallicity spectra.

5. OBSERVATIONS

HUT observed four stars that are appropriate for demonstrating the validity of our models. They are listed in Table 2.

The HUT instrument uses a 90 cm diameter f/2 primary mirror and a prime focus, near-normal-incidence, Rowland-circle grating spectrograph to obtain spectrophotometry from 820 to 1840 Å in first order. The detector consists of a microchannel plate coupled to a phosphor intensifier that is read by a Reticon into 2048 pixels. A complete description of the instrument and its performance is given in Davidsen et al. (1992). Modifications and the resulting performance and calibration for the Astro-2 mission are described in Kruk et al. (1995). The final Astro-1 calibration of HUT is presented in Kruk et al. (1996). For the purposes of this paper, it is important to note that the HUT calibration is very secure and is based on both laboratory measurements and observations of white dwarf standards. Uncertainties in throughput are less than 5%.

We observed each of the four stars through a 20″ slit, giving variable resolution (2–4 Å) spectra with nonlinear pixel spacing of $\approx$0.51 Å. Each of the stars was observed in

TABLE 2

HUT OBSERVATIONS AND MODELS

Parameter	HD 188665	PG 1710+490	PG 0839+399	BD +75°325
Spectral Type	B5 V[a]	sdB[b]	sdB[b]	O5pvar[c]
V (mag)	5.15[c]	12.02[d]	14.03[d]	9.55[c]
$B-V$ (mag)	−0.14[c]	−0.24[d]	−0.29[d]	−0.36[c]
Observed time (s)	1422	448	866	1612
Model $T_{\rm eff}$ (K)	17,000[a]	29,900[b]	36,100[b]	55,000[e]
Model log g	4.0[a]	5.7[b]	5.9[b]	5.3[e]
Model $E(B-V)$	0.07	0.03	0.04	0.03

[a] Buss et al. 1995.
[b] Saffer et al. 1994.
[c] SIMBAD.
[d] Wesemael et al. 1992; Turner 1990; Green, Schmidt, & Liebert 1986.
[e] Hubeny et al. 1991.

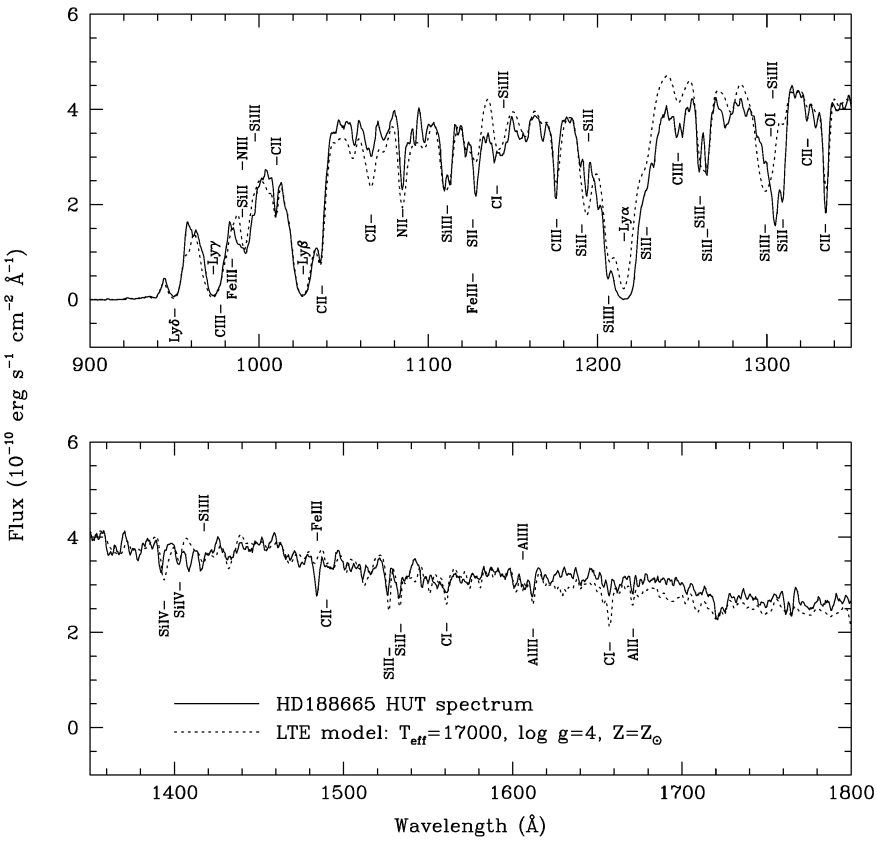

FIG. 2.—Data (*solid curve*; smoothed by a three-bin = 1.5 Å boxcar) from a HUT observation of the B5 V main-sequence star HD 188665 fairly coincides with most wavelength regions of an LTE synthetic spectrum (*dotted curve*). The largest discrepancies, like those at 1250 Å, are most likely due to inadequate opacity in the model. The discrepancies at 1216 and 1304 Å are due to detector degradation from airglow. Strong absorption features in the model (*labeled*) reflect deviations from solar abundances in the HD 188665 atmosphere and some imprecision in the model. The model is reddened with $E(B-V) = 0.07$; it does not include any contribution from airglow, which should be negligible with respect to the bright HD 188665 spectrum observed though a small aperture.

a different combination of telescope apertures, chosen to limit the fluxes incident on the detector to acceptable values. HD 188665 was observed with a 50 cm^2 aperture, PG 1710+490 was observed in both 5120 and 2160 cm^2 apertures, PG 0839+399 was observed in the 5120 cm^2 aperture, and BD +75°325 was observed in both the 20 and 50 cm^2 apertures. All of the data were flux calibrated and corrected for flat-field features, and the data for the two brightest objects (HD 188665 and BD +75 325) were also corrected for loss of counts due to detector deadtime. The final spectra, shown in Figures 2, 3, 4, and 5, were not corrected for airglow emission or interstellar extinction. Considerable degradation of the detector response at 1216 and 1304 Å, caused by exposure to bright airglow emission (Lyα and O I, respectively), artificially depresses the spectra in these wavelength regions.

6. TESTS OF THE MODELS

6.1. *Comparison to HUT Observations*

Table 2 also lists the parameters of the models that we compare to each of the four stars observed with HUT. Because the stars span a range in temperature and gravity, the models demonstrate the different regimes of our grid. The model parameters used were taken from the literature and have not been varied to produce optimum fits to the data.

For the three hottest stars, we generated new model atmospheres and spectra (not from our grid) that match exactly the temperature and gravity of those stars, as given in the literature. In all other aspects, these models are exactly the same as those in our grid, and thus demonstrate the validity of the grid points for matching a given set of parameters ($T_{\rm eff}$, log g). The coolest star (HD 188665) has a temperature below 20,000 K and thus falls in the regime in which we use Kurucz (1993) atmospheres. Hence, for HD 188665, the synthetic spectrum is from our grid of models, taking the point that most closely matches the true parameters of the star. All four models assume solar abundances, although it is known that the stars observed have atmospheres with nonsolar abundances (Hubeny, Heap, & Altner 1991; Saffer et al. 1994; Wolff & Heasley 1985).

While it would be possible to fit the atmospheric parameters (temperature, gravity, and abundance) of the four HUT stars, we stress that these models have the same simple characteristics as those in our grid. We did fit the extinction to each of the stars, using the extinction parameterization of Cardelli, Clayton, & Mathis (1989) and assuming $R_V = 3.1$. The extinction is quite low [$E(B-V) \leq 0.07$] for each of the four HUT stars, as shown in Table 2. We also applied interstellar absorption from neutral hydrogen to each of the four models, assuming a column density of log $N_{\rm H}$ [cm^2] = 18.0 with a Doppler b-parameter of 10 km s^{-1} and a temperature of 10 K. The true column density may be somewhat higher.

Figures 2, 3, 4, and 5 show the four HUT stars and their respective models. For the purposes of the figures, we convolve the synthetic spectra to match the HUT data, which

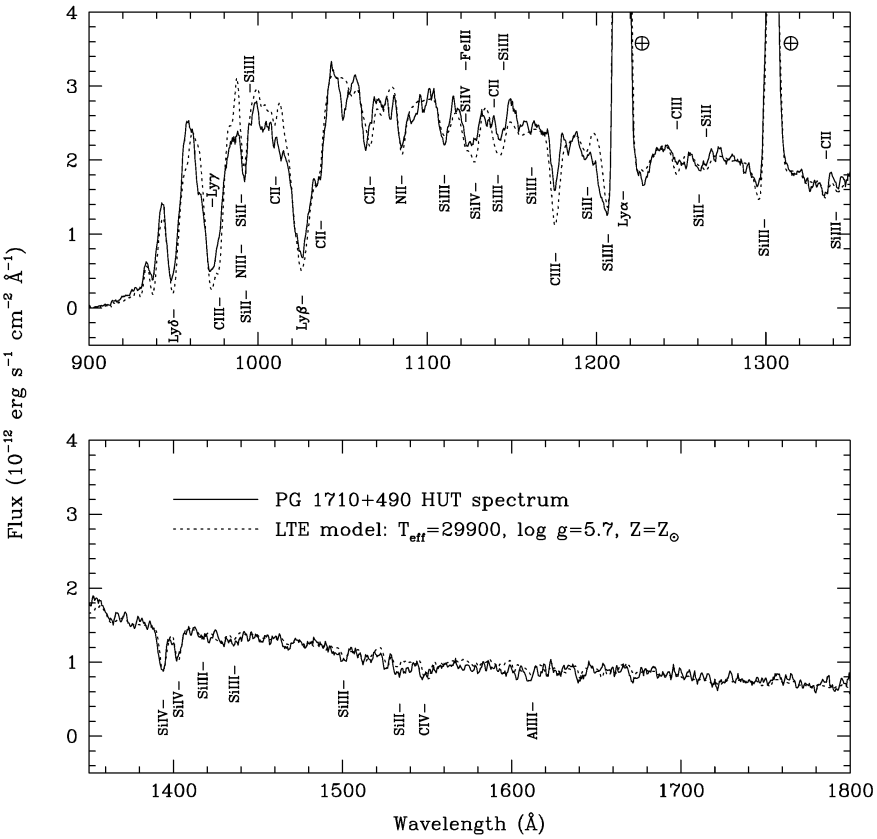

FIG. 3.—Data (*solid curve*; smoothed by a three-bin boxcar) from a HUT observation of the hot subdwarf PG 1710+490 agrees fairly well with a model LTE spectrum (*dotted curve*). Discrepancies in the Lyman lines are apparent in the plot, however. Metal abundance in the star varies from solar, as evidenced by the discrepancies between absorption features in the model (*labeled*) and those in the data. The model is reddened with $E(B-V) = 0.027$ and has a contribution from a scaled "typical" day airglow spectrum, which respectively fills the Lyα and Si III stellar absorption lines with Lyα and O I airglow (*circled cross*).

have both variable resolution (2–4 Å for point sources) and (slightly) variable pixel spacing. Overall, the matches between the models and the data are quite good. The strengths of the lines in the models are not expected to be a perfect match to the data, since these stars have nonsolar abundances in their atmospheres and the models are not completely accurate. As mentioned above, airglow lines caused detector degradation at 1216 and 1304 Å, giving false absorption features in the HUT data. However, an obvious problem is a mismatch in the strength of the Lyman series, which is discussed further below.

The extinction parameterization of Cardelli et al. (1989) does not extend below 1000 Å. We have extrapolated it to the Lyman limit (912 Å), but the uncertainty in this extrapolation may cause some of the discrepancy between the models and data at the shortest wavelengths.

Although the spectral type of HD 188665 is well documented as B5 V, Buss, Kruk, & Ferguson (1995) found that the effective temperature determined from the FUV spectral energy distribution (SED) is a somewhat hotter 17,000 K. While we use Figure 2 to demonstrate the accuracy and the problems of a 17,000 K model, we found that an 18,000 K model with the same surface gravity fits the HUT data somewhat better. The largest discrepancies, like the one apparent at 1240 Å, are most likely due to inadequate opacity in the model; more continuum opacity with less extinction could bring the model into better agreement with the data.

PG 1710+490 and PG 0839+399 are both hot subdwarfs (Saffer et al. 1994) and are expected to show a redistribution of the metals from gravitational settling in their stellar atmospheres. The line strengths of the strongest features in the PG 1710+490 data and model (Fig. 4) are listed in Table 3. Line blanketing in the FUV makes the determination of a continuum difficult and translates into difficulty in making equivalent width measurements. Because of this difficulty, the equivalent widths listed for the PG 1710+490 data were measured by adopting the continuum level from the LTE model, with the lines in question removed and then fitting Gaussian absorption features via χ^2 minimization. This method isolates the contribution of a specific species to the line, even when more than one species may contribute. However, it is important to note that this procedure is different from the standard way of measuring equivalent widths, in that we do not define local continuum regions on either side of the features but rather rely on the overall normalization of the model spectrum. Mismatches between the model continuum and the true continuum could thus introduce systematic errors in the measurements. Also, departures of the line centers from their model velocities (i.e., because of winds) can affect the measurements. As is evident in the table, C may be somewhat depleted relative to solar abundance, while Si and N appear to be at approximately solar abundances. The depletion of metals is much greater in the HUT spectrum of PG 0839+399 (Fig. 4), where both Si and C are depleted relative to solar abun-

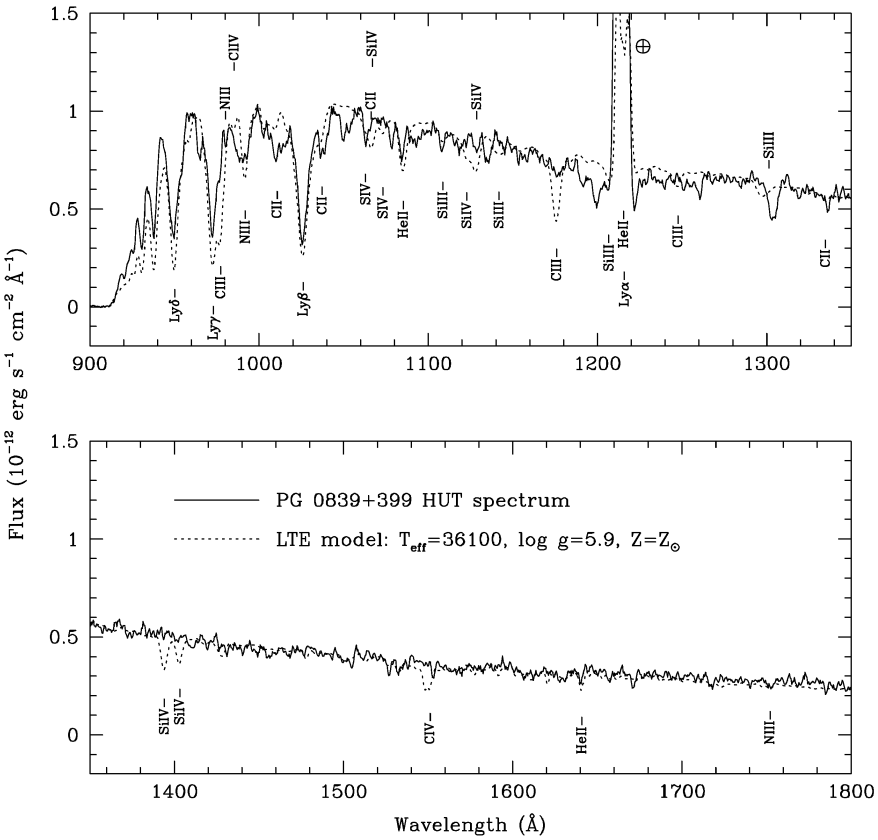

FIG. 4.—Data (*solid curve*; smoothed by a three-bin boxcar) from a HUT observation of the hot subdwarf PG 0839+399, overplotted with a model LTE spectrum (*dotted curve*). Discrepancy in the Lyman lines is stronger than the discrepancy in PG 1710+490. Metal abundances in the star are nonsolar. The model is reddened with $E(B-V) = 0.04$ and has a contribution from a scaled "typical" night airglow spectrum, which respectively fills the Lyα and Si III stellar absorption lines with Lyα and O I airglow (*circled cross*). Detector degradation from airglow causes the apparent absorption at 1304 Å.

TABLE 3

STRONG ABSORPTION FEATURES IN SYNSPEC SPECTRA AND HUT DATA

	EQW (Å)			
	PG 1710+490		$T_{\rm eff}$ = 30,000 K, log g = 5	
FEATURE	HUT Data[a]	LTE Model[b]	TLUSTY Atmosphere[c]	Kurucz Atmosphere[d]
Lyϵ λ938	7.3 ± 1.7	8.2	7.4	6.2
Lyδ λ950	9.0 ± 2.3	10.1	7.0	5.9
Lyγ λ973	12.4[e] ± 2.2	11.4	7.2	5.9
C III λ977	0.9[e] ± 1.5	3.2	5.0	4.6
N III λ991	3.6 ± 0.3	2.5	2.1	1.8
Lyβ λ1026	10.8 ± 0.5	10.8	7.3	6.0
C II λ1036	1.6 ± 0.3	1.8	1.4	1.0
N II λ1085	1.6 ± 0.6	0.8	0.7	0.6
Si III λ1111	1.5 ± 0.2	1.6	1.5	1.1
C III λ1176	2.2 ± 0.2	4.1	3.9	3.6
Si III λ1206	...	2.7	2.6	1.8
Lyα λ1216	...	10.2	6.7	5.5
Si III λ1300	...	2.9	2.9	2.0
Si IV $\lambda\lambda$1394, 1403	4.4 ± 0.4	4.0	4.3	4.2
C IV $\lambda\lambda$1548, 1551	1.5 ± 0.2	1.2	1.7	2.3

[a] Equivalent widths in the data are measured by adopting the continuum level from the model, with the line in question removed (see text). The reported errors in the second column are simply from count statistics and do not take the systematic uncertainties into account.

[b] TLUSTY atmosphere and SYNSPEC spectrum with T = 29,900 K and log g = 5.7.

[c] TLUSTY atmosphere used in SYNSPEC.

[d] Kurucz 1993 atmosphere used in SYNSPEC.

[e] Lyγ and C III are heavily blended in the HUT spectrum.

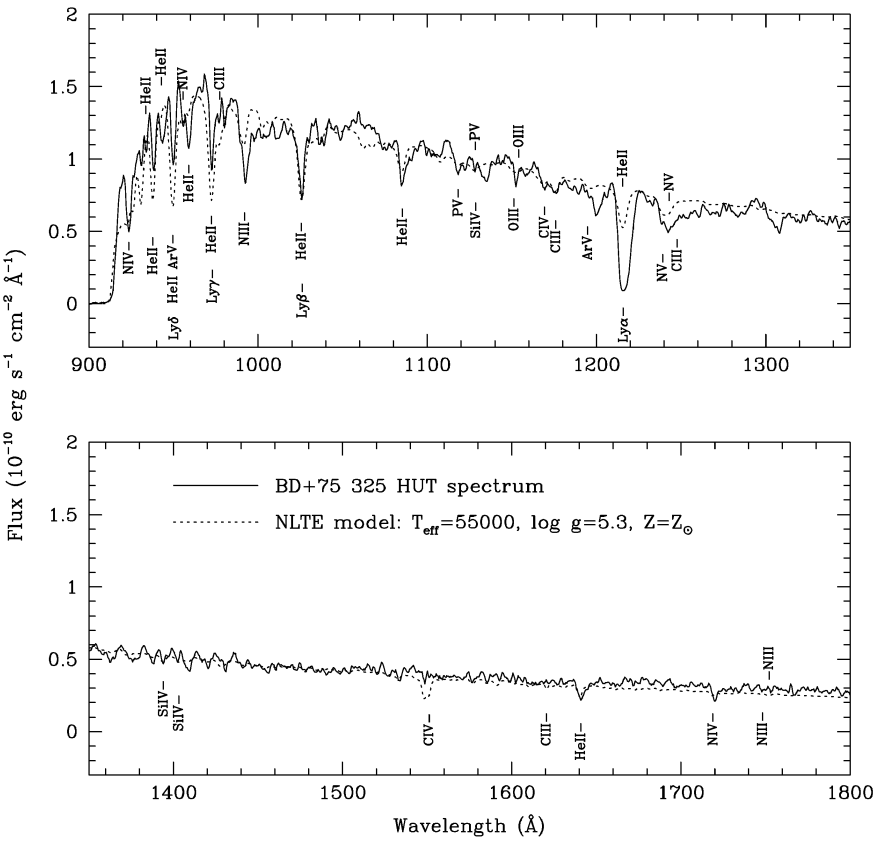

FIG. 5.—Data (*solid curve*; smoothed by a three-bin boxcar) from a HUT observation of the early O star BD +75°325, overplotted with a model NLTE spectrum (*dotted curve*). Discrepancy in the Lyman lines is stronger than the discrepancy in 1710+490. Absorption features (*labeled*) show that the metal abundance in the star differs from solar. The model is reddened with $E(B-V) = 0.03$ and but has no contribution from airglow, which should be negligible in this observation. Detector degradation is apparent in the HUT data at 1216 and 1304 Å.

dances. Although we did not perform a χ^2 fit of the abundances, we found that a closer match to the HUT PG 0839+399 data could be found with a synthetic spectrum having C and Si at 0.03 solar abundance and N at 0.25 solar abundance. In general, helium is expected to be overabundant in sdO stars and underabundant in sdB stars, while in both types of stars, C and Si appear underabundant, and N appears normal (Saffer & Liebert 1995). Blair, Long, & Raymond (1996) also analyzed PG 0839+399 using the TLUSTY code with simple H and He model atmospheres. They found that a hotter $T_{\rm eff}$ of 40,300 K produced better agreement in the Lyman lines and that the inclusion of H_2 absorption improved their fit shortward of 1100 Å. Our own grid also demonstrates better agreement for hotter temperatures (see discussion in § 6.3).

The early O star BD +75°325 shows stronger than expected N absorption but appears underabundant in C and Si. Although the synthetic spectrum fairly approximates the HUT data, it is apparent that the inaccuracies of the models are increasing at the shortest wavelengths for higher temperatures. BD +75°325 has metal abundances that differ significantly from solar and considerably enriched He abundance (Hubeny et al. 1991 and references therein).

6.2. *Comparison to Kurucz Models*

We compare three of the synthetic spectra from our grid to three spectra from the grid of Kurucz (1992) in Figure 6. Unlike real stars, the Kurucz spectra have precisely known metal abundances; the comparisons demonstrate that the approximations we have made in constructing higher resolution spectra do not significantly distort the continuum shape, even though Kurucz includes more sources of continuum opacity and a larger line list when generating his synthetic spectra. We also compare one of our model atmospheres to one from the Kurucz (1993) grid in Figure 7 in order to demonstrate the effect our simplifications have on the atmospheric structure.

The temperatures and gravities of the synthetic spectra were chosen to complement the comparisons to stars in the previous section. The metal abundances are at 0.1 solar abundance. Figure 6 shows good agreement in the two hotter comparisons but weaker agreement for the coolest model. The coolest synthetic spectrum is derived from a Kurucz (1993) model atmosphere, since it has an effective temperature below 20,000 K. The accuracy of our synthetic spectra becomes worse as one moves to effective temperatures of 10,000 K and below because of a lack of appropriate continuum and line opacity in the calculations. However, stars in this temperature range contribute an insignificant amount of the FUV flux from elliptical galaxies. For these reasons, we do not compute synthetic spectra below 10,000 K. In general, models of higher metallicity ($Z = Z_\odot$) show somewhat less agreement than the spectra shown in Figure 6, while models of lower metallicity ($Z = 0.01\,Z_\odot$) show better agreement.

Because our simple model atmospheres do not include the effects of line blanketing when computing the atmospheric structure, there are differences in this structure when comparing our atmospheres to those of Kurucz (1993).

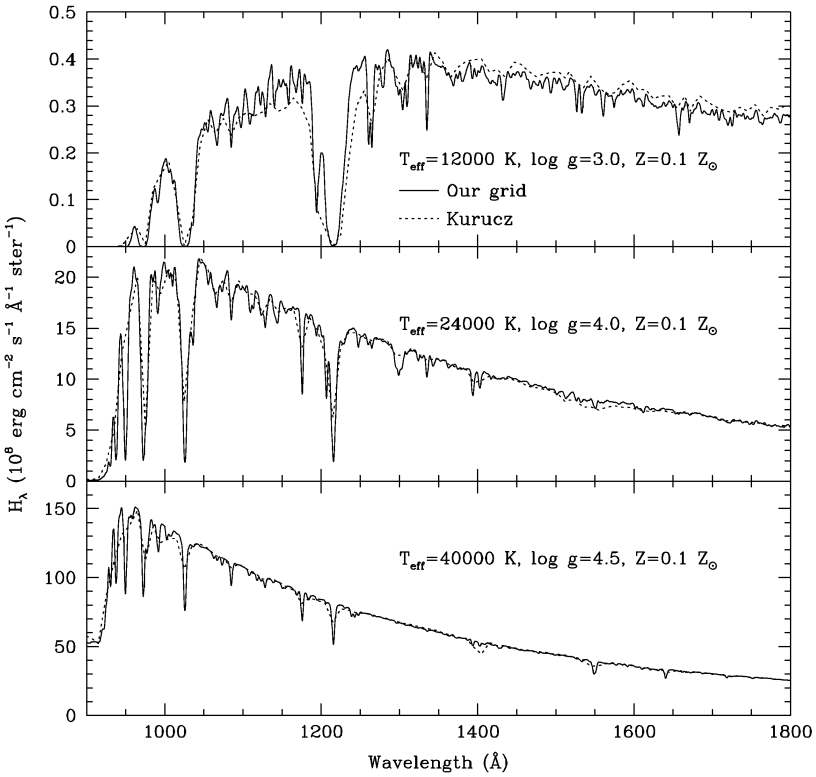

FIG. 6.—Three LTE spectra from our grid (*solid curve*; 3 Å resolution) are compared to three spectra from the Kurucz (1992) grid (*dashed curve*; 10 Å resolution). The metallicity $Z = 0.1\ Z_{\odot}$. At higher metallicity ($Z = Z_{\odot}$), discrepancies between our grid and the Kurucz grid are somewhat worse. At lower metallicity ($Z = 0.01\ Z_{\odot}$), agreement between our grid and the Kurucz grid is better.

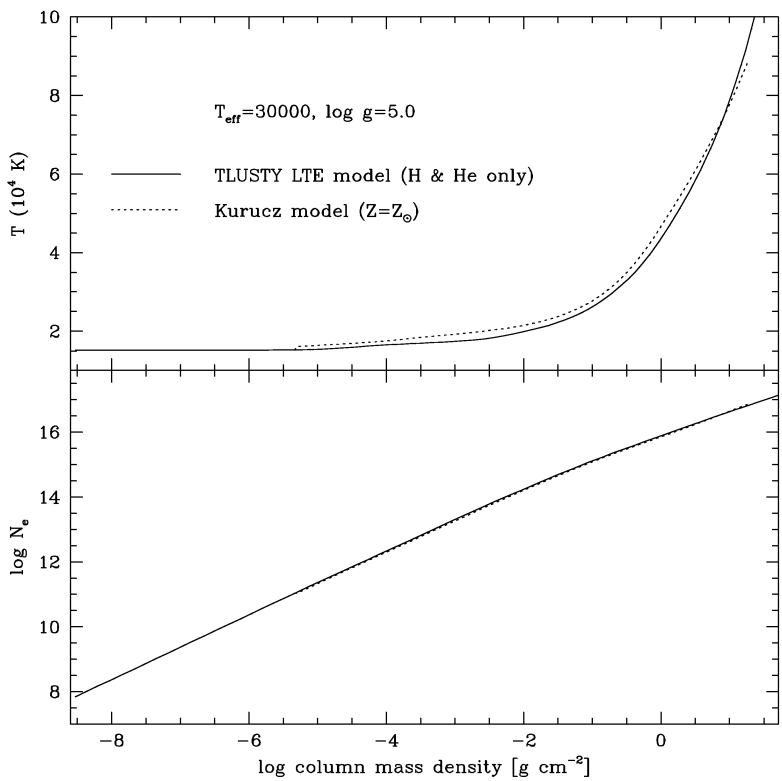

FIG. 7.—Our model atmospheres show structural differences when compared to atmospheres from the Kurucz (1993) grid. These differences are due to the lack of line blanketing in the construction of our model atmospheres. The discontinuity at the surface of the Kurucz (1993) atmosphere is a real feature in the model.

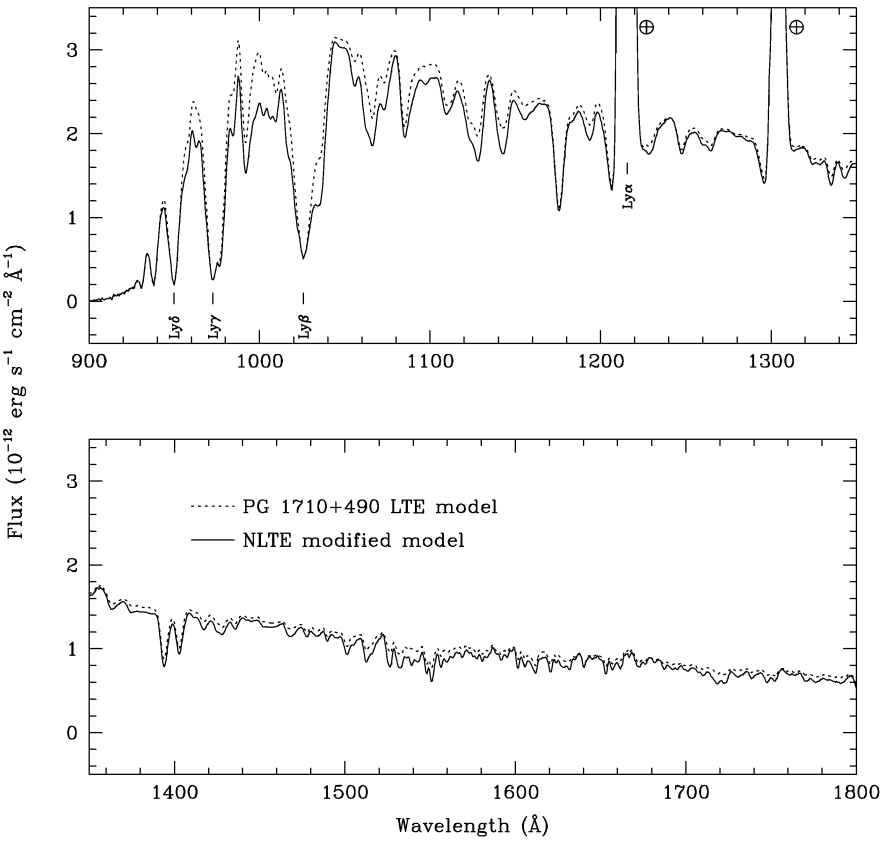

FIG. 8.—A more complex NLTE model for PG 1710+490 (*solid curve*), when compared to the simple LTE model from Fig. 3 (*dotted curve*), rules out several possible explanations for the Lyman series discrepancy that appears in Figs. 2, 3, 4, and 5. Although the NLTE model has reduced He abundance, higher turbulent velocity (10 km s^{-1}), EUV and FUV continuum opacity from elements heavier than He, and Stark broadening in Lyα–Lyδ for the atmosphere calculation, the cores of the Lyman lines are still as deep as those in the LTE model. Both models include a scaled airglow contribution, are reddened with $E(B-V) = 0.027$, and are normalized to the HUT data. We also note that the NLTE model demonstrates that the simplifications in our models introduce only small inaccuracies at this temperature.

Figure 7 shows the comparison for $T_{\rm eff} = 30{,}000$ K and log $g = 5$. As explained in § 3.2, the TLUSTY atmosphere is of pure H and He, while the Kurucz (1993) atmosphere includes heavier elements at solar abundance. Both are calculated over somewhat different bounds of column mass density, but where they overlap, our temperature is always somewhat lower and our electron density is very slightly higher. We note that our model atmospheres start at a smaller optical depth and extend to greater optical depth than the Kurucz (1993) models; this is reflected in the horizontal extent of the curves plotted in Figure 7. Computing our atmospheres with the same bounds in optical depth (and column mass density) as the Kurucz (1993) atmosphere does not significantly change our temperature structure.

We used the two atmospheres in Figure 7 as input for SYNSPEC, produced synthetic spectra, and then compared the line strengths of the strongest lines (Table 3), assuming solar metallicity in the spectrum derived from our own TLUSTY atmosphere. In most cases, lines derived using our atmosphere are somewhat stronger than those derived using the Kurucz (1993) atmosphere. Near the surface of the atmosphere, our temperature is only about 1000 K cooler than that in the Kurucz (1993) atmosphere. Since the strongest lines, like the Lyman series, are formed very near the surface of the atmosphere, the small difference in temperature structure probably explains part, but not all, of the Lyman series problem described below.

6.3. *The Lyman Series Problem*

Our models consistently show stronger Lyman lines than those present in the HUT data. Although we explored many possible explanations for the discrepancy (other than changing the effective temperature or gravity), we have yet to correct this problem, and it is the most glaring limitation to our models. Allowing the temperature and gravity to vary as free parameters in fits to the data can produce agreement between the Lyman line cores in the data and those in the models; a model atmosphere with an effective temperature that is several thousand degrees hotter than the value in the literature, in combination with a larger extinction, produces a better fit. However, the temperatures and gravities found in the literature are well established. For example, the parameters deduced from Balmer line fitting for PG 1710+490 and PG 0839+399 have errors of 500 K in $T_{\rm eff}$ and 0.12 dex in log g (Saffer et al. 1994).

Instrumental effects can be ruled out as well. As shown by Kruk et al. (1995), HUT's effective area is fairly smooth across the Lyman series wavelength region. Also, the saturated Lyman lines in the HD 188665 HUT spectrum (Fig. 2) demonstrate that the lines are not filled with scattered light. Finally, the white dwarfs in Kruk et al. (1995) show good agreement between the Lyman lines in the models and those in the HUT data. The hot DA white dwarfs that were used to calibrate HUT were chosen because they are simple

objects that are relatively easy to model and understand. Their atmospheres consist of nearly pure hydrogen, are very nearly plane-parallel, have no detectable winds, and do not significantly depart from LTE (Finley 1993).

Our first thought was that airglow emission from neutral H in Earth's atmosphere partially filled the lines in the data, but as Figure 3 shows, the inclusion of airglow in the model for PG 1710+490 does not bring the model into agreement with the data. Other factors that could affect the model are the inclusion of heavier elements in the model atmosphere; a larger turbulent velocity; NLTE effects; the use of Stark broadening in the atmosphere calculation; and the depletion of He in the atmospheres of hot subdwarfs. To demonstrate the cumulative effect of all of these factors, Figure 8 compares the simple LTE model for PG 1710+490 with a more sophisticated NLTE model. The NLTE model explicitly includes all of the atomic energy levels and opacities of the LTE model (from H I, He I, and He II) and also 26 levels of C III and 23 levels of N III (with their respective opacities and transitions). Elements with atomic number $Z \leq 30$ (other than H, He, C, and N) contribute to the total number of particles and the total charge (but not to the opacity), assuming LTE ionization balance. The turbulent velocity has been increased from 2 to 10 km s^{-1} in the NLTE model, and the first four Lyman lines include Stark broadening in the atmosphere calculation. The abundances of all elements are taken to be solar in the NLTE model, except for He, which is at $Y = 0.006$ (Saffer et al. 1994). As is evident from Figure 8, the Lyman line cores are unchanged in the NLTE model. The cores of these strongest lines are formed very high in a stellar atmosphere, where small changes in the physical structure of the atmosphere are emphasized. It may therefore require an extremely complex model atmosphere (that includes line blanketing and perhaps stellar winds) to calculate the strongest lines in these stellar spectra accurately. While the more complex model does not solve the Lyman series problem, the comparison in Figure 8 serves to demonstrate that many of the simplifications we have assumed in our grid do not result in large errors in the final synthetic spectra.

7. MAJOR SOURCES OF LINE OPACITY

Among the many experiments one can perform using the Hubeny (1988) code is the isolation of specific elements in synthetic spectra. At HUT resolution in the FUV, nearly all features are blends. It is not always obvious from line lists which features to use as abundance, temperature, or gravity indicators. To make this more evident, we computed subsets of solar metallicity synthetic spectra using modified line lists that are missing lines from one of four elements: C, N, Si, or Fe. For each of these elements, we computed synthetic spectra with and without the presence of the element and formed the ratio of these spectra to produce the absorption spectrum of that element alone (Figs. 9, 10, 11, and 12). C, N, Si, and Fe contribute the bulk (roughly 75%) of the FUV line opacity in the temperature range of 25,000 K $\leq T_{\rm eff} \leq$ 35,000 K and gravity range of $4.0 \leq \log g \leq 6.0$; this parameter space is relevant to the likely sources of FUV

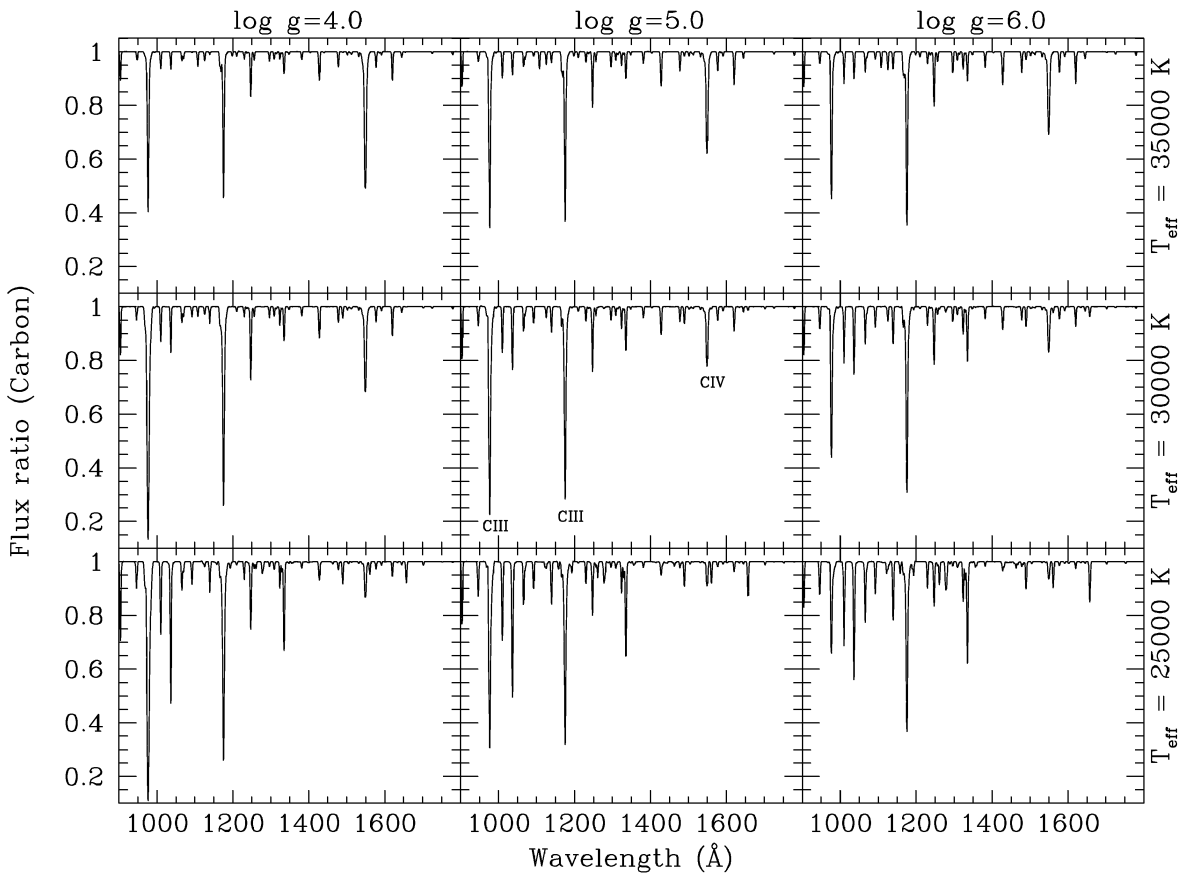

FIG. 9.—Absorption spectrum of carbon in the HUT wavelength range shows those features (*labeled*) that should be useful in determining the temperature, surface gravity, and metallicity of the dominant stellar components in early-type galaxy spectra. Plotted at 3 Å resolution is the ratio of two spectra: a spectrum with carbon divided by one without carbon, for nine different combinations of temperature and surface gravity, assuming solar metallicity $[N(C)/N(H) = 3.68 \times 10^{-4}]$.

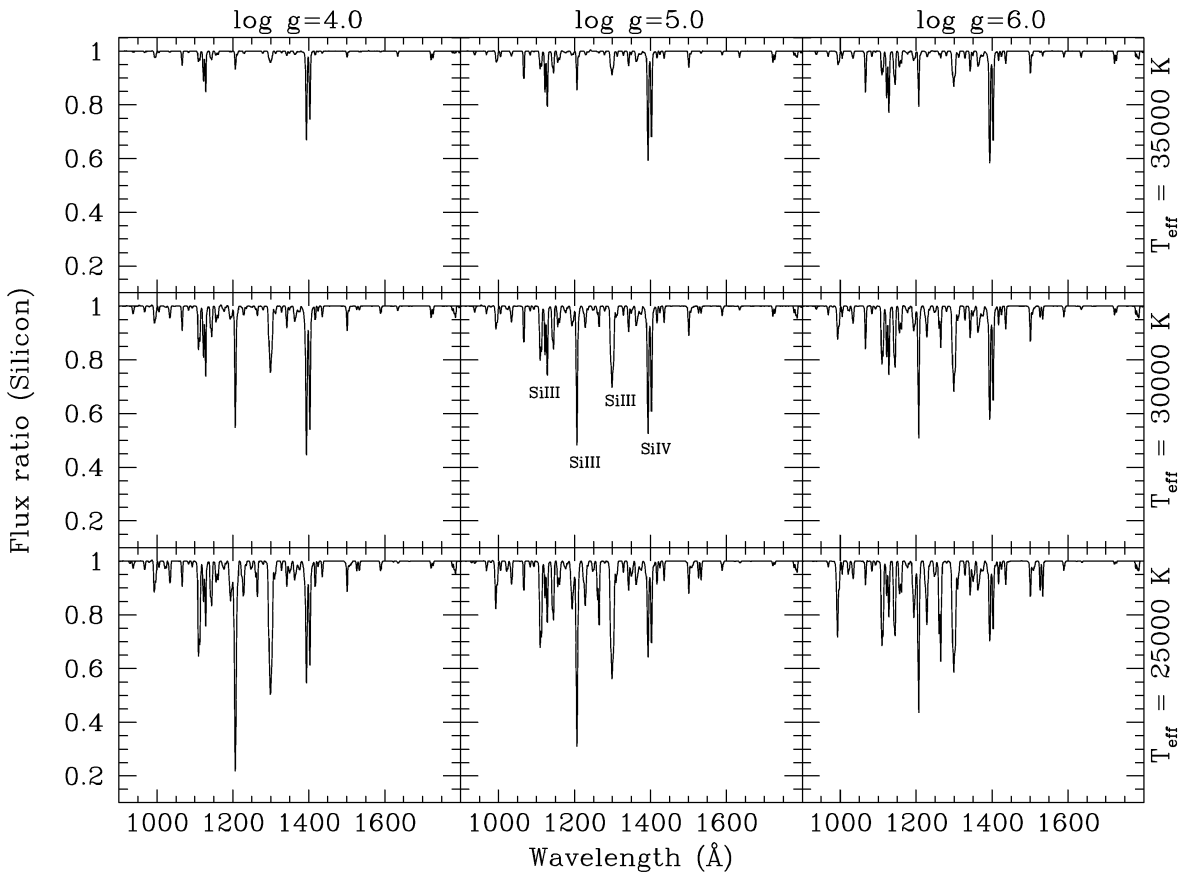

FIG. 10.—As in Fig. 9, but for silicon [N(Si)/N(H) = 3.51 × 10^{-5}]. The silicon absorption spectrum shows lines almost as strong as those in the carbon spectrum and several features (*labeled*) that should be useful in characterizing a stellar population.

flux in early-type galaxies. Of the 10 most abundant elements in the solar atmosphere (O, C, N, Ne, Si, Mg, S, Fe, Ar, and Al), O, Ne, Mg, S, Ar, and Al do not contribute many strong lines in the FUV at these temperatures and gravities.

The strong lines in Figures 9, 10, 11, and 12 offer a way of estimating the temperatures, gravities, and metallicities of the dominant stellar components contributing to the FUV flux in early-type galaxies. Their use is limited, since the galaxy spectrum will be a composite of many different stars, yet these singular models offer an insight that complements that offered by composite model spectra. There are subtleties in the figures that go beyond the general trend for higher ionization states to exist at higher temperatures and lower surface gravities.

7.1. *Carbon Lines*

Other than the Lyman series, our models show that carbon lines (Fig. 9) are the strongest lines likely to appear in the spectra of HB stars and elliptical galaxies. Two of these features are always extremely strong: C III λ977 and C III λ1176. As such, they might be measurable in relatively low signal-to-noise ratio spectra of galaxies, and their relative strengths are a strong indicator of surface gravity. In practice, however, such an indicator will be difficult to measure, since the Lyγ λ973 absorption overlaps with that of C III λ977.

A third feature, C IV λλ1548, 1551, is strong at higher temperatures and weaker gravities. Ferguson et al. (1991) have argued that the lack of detectable C IV in the Astro-1 observations of galaxies M31 and NGC 1399 shows that young, massive stars cannot be the dominant contributors to the FUV flux in these galaxies. Brown et al. (1995) made the same point regarding the six galaxies observed with HUT on Astro-2.

The C III λ1176 feature is also useful for estimating the carbon abundance. Figure 9 demonstrates that its strength is relatively insensitive to changes in temperature and gravity; in this regime, the equivalent width varies from 2.3 to 4.3 Å.

7.2. *Silicon Lines*

Contributing lines almost as strong as those of carbon, silicon has several features that may help characterize the stellar populations in early-type galaxies. Although not the strongest feature, Si IV λλ1394, 1403 is strong at all of the temperatures and gravities shown in Figure 10; it is useful as an abundance indicator.

Si III λ1206 is a very strong indicator of temperature but is of limited use because of its proximity to Lyα λ1216. The same can be said of the Si III lines near 1300 Å. Although sensitive to temperature, they are near the O I λ1304 airglow lines that have caused detector degradation in that wavelength region.

If C IV implies a dominant temperature component near 25,000 K, then the cluster of strong Si III lines from 1108 to 1113 Å should be indicative of the Si abundance. Or, if the Si IV λλ1394, 1403 indicates that Si is near solar abundance, these Si III lines could be indicative of the temperature.

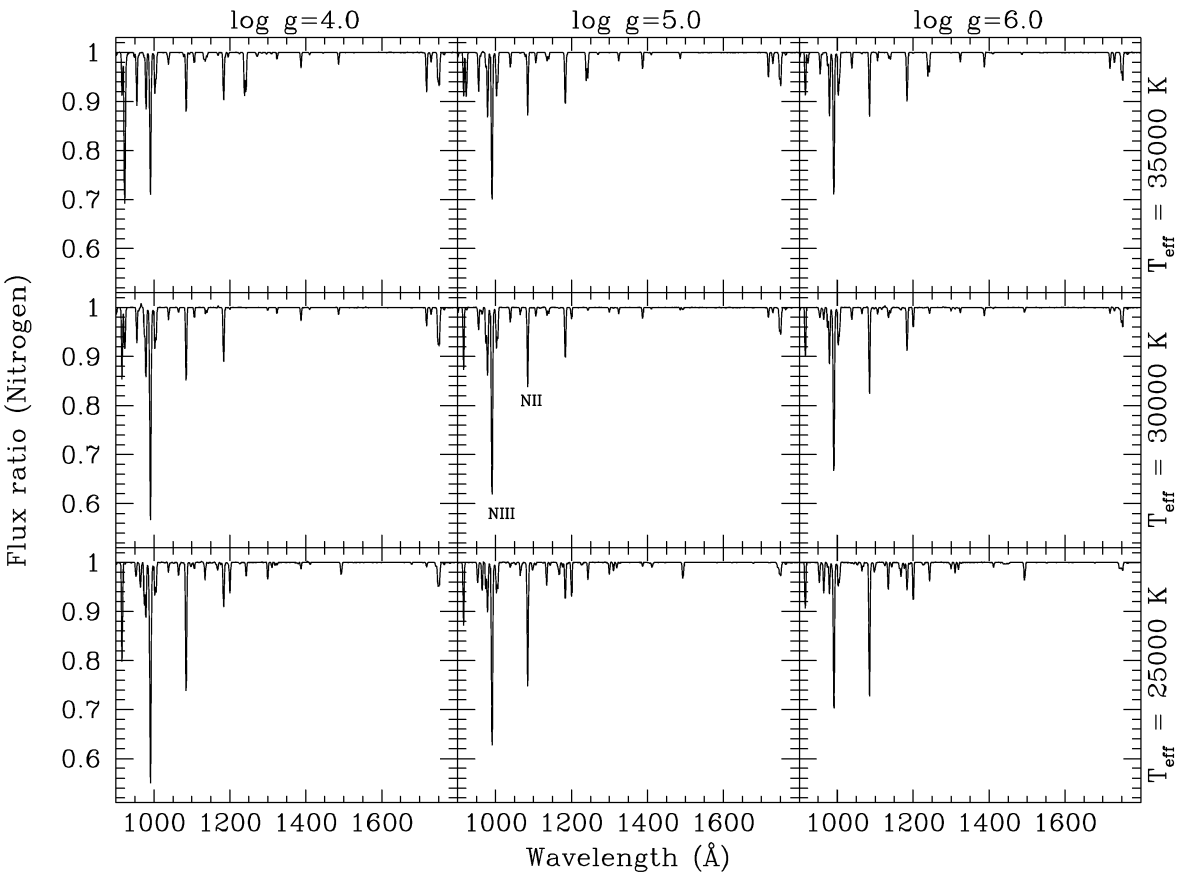

FIG. 11.—As in Fig. 9, but for nitrogen [$N(N)/N(H) = 1.14 \times 10^{-4}$]. While the nitrogen absorption spectrum has only a few lines (*labeled*) in the HUT range at these temperatures and gravities, those lines will provide a useful diagnostic for analyzing the Astro-2 galaxy spectra.

7.3. *Nitrogen Lines*

Although there are not many lines from nitrogen in Figure 11, the few that are present will be useful. The cluster of N III lines near 991 Å is strong throughout the range of temperature and gravity shown and will be useful as an abundance indicator. A group of N II lines at 1085 Å is fairly sensitive to temperature while being almost completely insensitive to gravity, which allows one to separate the two effects.

7.4. *Iron Lines*

Iron is a well-known source of many lines in the FUV, and Figure 12 demonstrates how its absorption lines depress the flux in the HUT wavelength region. At all temperatures and gravities, Fe absorption makes it difficult to define a region that can be used to measure the continuum level in these spectra. Only in the range 1200–1400 Å does the Fe line blanketing decrease to a small ($\approx$2%) effect.

Toward the shorter wavelengths in the HUT range, the dominant source of line blanketing comes from Fe III. For example, in the center panel of Figure 12, Fe II accounts for 7% of the line opacity from 900 to 1200 Å, Fe III accounts for 92%, and Fe IV accounts for 1%. This blanketing becomes weaker at higher temperatures as more Fe moves to the higher ionization stages, and the effect is to exaggerate the trend of stellar spectra to show steeper slopes at hotter temperatures.

Toward the longer wavelengths in the HUT range, the dominant source of line blanketing still comes from Fe III, but it is a reduced contribution: in the center panel of Figure 12, Fe II contributes to 6% of the line opacity in the region 1500–1800 Å, while 67% comes from Fe III and 27% from Fe IV. Since the opacity is now shared more equally between Fe III and Fe IV, the line blanketing in this region is less sensitive to changes in temperature and gravity as compared to the line blanketing at shorter wavelengths.

Thus, Fe lines change the continuum shape of HUT spectra, creating a pseudocontinuum that can make spectra look "hotter" for lower Fe abundance or "cooler" for greater Fe abundance. The effects are certainly large enough to be detectable in the galaxy spectra.

8. CONCLUSIONS

We have computed a grid of model atmospheres and synthetic FUV spectra that span a range of 10,000 K $\leq T_{\rm eff} \leq$ 250,000 K and $2 \leq \log g \leq 8.5$, with three metallicities: $Z = Z_\odot$, $Z = 0.1\ Z_\odot$, and $Z = 0.01\ Z_\odot$. Although our grid of synthetic spectra has limitations (e.g., the inaccuracy of the Lyman series), comparison to observations of four stars demonstrates that they are accurate enough to create composite model spectra for comparison to data from HUT early-type galaxy observations. They are most accurate in the temperature regime below 60,000 K, and in this regime HB stars and their progeny are thought to provide the bulk of the FUV flux in early-type galaxies. Since these synthetic spectra match the HUT resolution and wavelength coverage, they will be valuable in characterizing the temperature, gravity, and abundances of the dominant

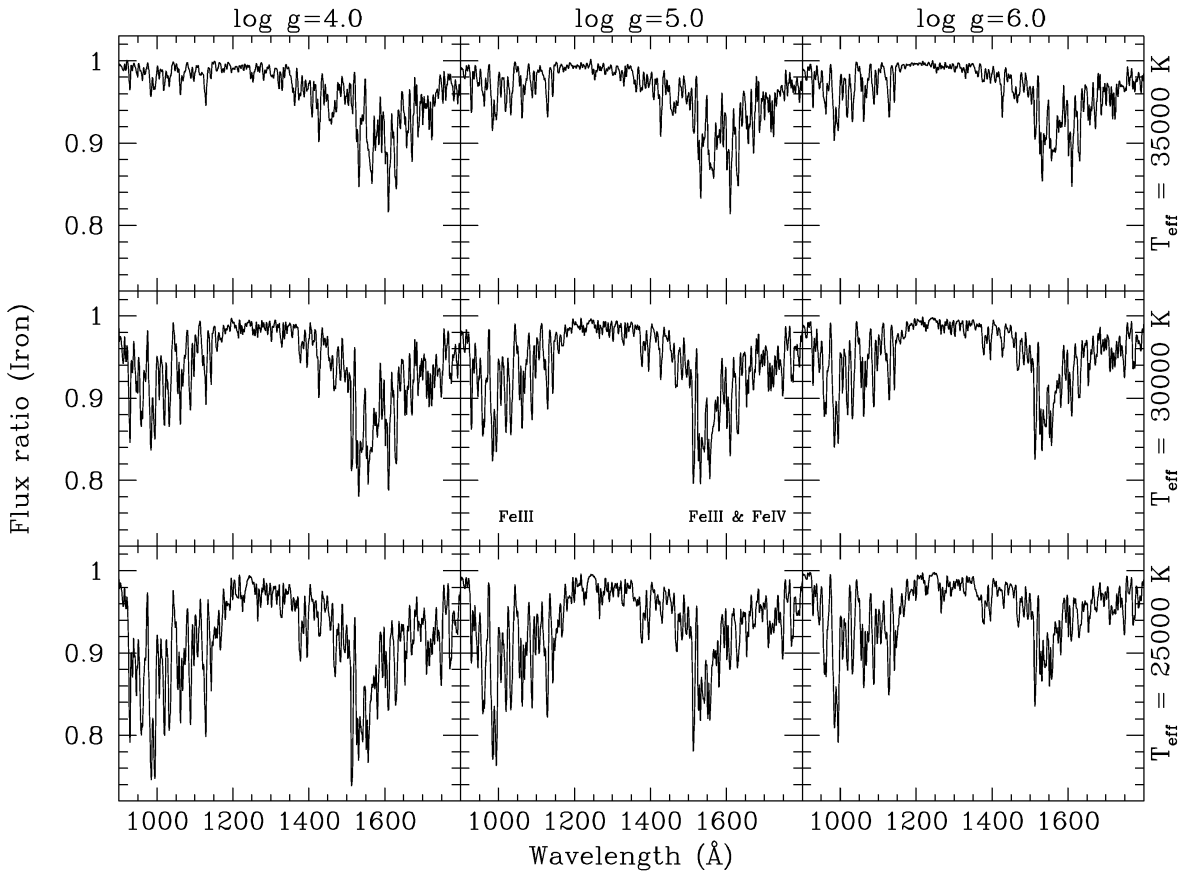

FIG. 12.—As in Fig. 9, but for iron [N(Fe)/N(H) = 2.49 × 10^{-5}]. The iron absorption spectrum depresses the continuum in two large regions of the HUT spectrum, creating a "pseudocontinuum." The line blanketing at short wavelengths is dominated by Fe III, while the blanketing at long wavelengths is due to Fe III and Fe IV.

stellar components in the eight galaxies observed on the Astro-1 and Astro-2 missions. Subsequent papers in this series will investigate both the absorption lines and the continuum shapes in the HUT FUV data, extending the work done by Ferguson et al. (1991), Ferguson & Davidsen (1993), and Brown et al. (1995).

This work was supported by NASA contract NAS 5-27000 to the Johns Hopkins University. We wish to thank Jeffrey Kruk for his assistance with the reduction of the HUT data. We are grateful to Ivan Hubeny for providing the latest versions of his code, advice on its use, and helpful comments. Rex Saffer gave helpful comments on the paper. Nicole Allard graciously provided the quasi-molecular hydrogen data used in our cool models.

REFERENCES

Allard, N. F., & Koester, D. 1992, A&A, 258, 464
Blair, W. P., Long, K. S., & Raymond, J. C. 1996, ApJ, 468, 841
Bressan, A., Chiosi, C., & Fagotto, F. 1994, ApJS, 94, 63
Brown, T. M., Ferguson, H. C., & Davidsen, A. F. 1995, ApJ, 454, L15
Buss, R. H., Kruk, J. W., & Ferguson, H. C. 1995, ApJ, 454, L55
Cardelli, J. A., Clayton, G. C., & Mathis, J. S. 1989, ApJ, 345, 245
Clegg, R. E. S., & Middlemass, D. 1987, MNRAS, 228, 759
Cunto, W., Mendoza, C., Ochsenbein, F., & Zeippen, C. J. 1993, A&A, 275, L5
Davidsen, A. F., et al. 1992, ApJ, 392, 264
Dorman, B., Rood, R. T., & O'Connell, R. W. 1993, ApJ, 419, 596
Ferguson, H. C., & Davidsen, A. F. 1993, ApJ, 408, 92
Ferguson, H. C., et al. 1991, ApJ, 382, L69
Finley, D. S. 1993, in Calibrating Hubble Space Telescope, ed. J. C. Blades & S. J. Osmer (Baltimore: STScI), 416
Green, R. F., Schmidt, M., & Liebert, J. 1986, ApJS, 61, 305
Hubeny, I. 1988, Comput. Phys. Comm., 52, 103
Hubeny, I., Heap, S. R., & Altner, B. 1991, ApJ, 377, L33
Hubeny, I., & Lanz, T. 1995, ApJ, 439, 875
Hubeny, I., Lanz, T., & Jeffery, C. S. 1995, SYNSPEC—A User's Guide
Kriss, G. A. 1994, in ASP Conf. Proc. 61, Astronomical Data Analysis Software and Systems III, ed. D. R. Crabtree, R. J. Hanisch, & J. Barnes (San Francisco: ASP), 437
Kruk, J. W., et al. 1995, ApJ, 454, L1
Kruk, J. W., et al. 1996, ApJ, submitted.
Kurucz, R. L. 1992, in IAU Symp. 149, The Stellar Populations of Galaxies, ed. B. Barbuy & A. Renzini (Dordrecht: Kluwer), 225
———. 1993, CD-ROM 13, ATLAS9 Stellar Atmosphere Programs and 2 km/s Grid (Cambridge: Smithsonian Astrophys. Obs.)
Lee, Y.-W. 1994, ApJ, 430, L113
Mihalas, D. 1970, Stellar Atmospheres (San Francisco: Freeman)
Moore, C. E. 1949, Atomic Energy Levels (Washington: US Dept. of Commerce)
Musgrove, A., Dalton, G. R., Martin, W. C., Saloman, E. B., Grant, C. S., & Eichhorn, G. 1996, NIST Atomic Spectroscopic Database (Gaithersburg: US Dept. of Commerce) http://aeldata.phy.nist.gov/mist_beta.html
Saffer, R. A., Bergeron, P., Koester, D., & Liebert, J. 1994, ApJ, 432, 351
Saffer, R. A., & Liebert, J. 1995, in Proc. of the 9th European Workshop on White Dwarfs, ed. D. Koester & K. Werner (Berlin: Springer), 221
Turner, D. G. 1990, PASP, 102, 1331
Vassiliadis, E., & Wood, P. R. 1994, ApJS, 92, 125
Wesemael, F., Fontaine, G., Bergeron, P., & Lamontagne, R. 1992, AJ, 104, 203
Wolff, S. C., & Heasley, J. N. 1985, ApJ, 292, 589